Double ionization of helium by 2-keV electrons in equal- and unequal-energy configurations

M. J. Ambrosio,[1,2] D. M. Mitnik,[1,2] A. Dorn,[3] L. U. Ancarani,[4] and G. Gasaneo[2,5]

[1]*Instituto de Astronomía y Física del Espacio (CONICET–UBA), Casilla de Correo 67-Sucursal 28 (C1428ZAA), Buenos Aires, Argentina*
[2]*Consejo Nacional de Investigaciones Científicas y Técnicas, Argentina*
[3]*Max-Planck-Institut für Kernphysik, Saupfercheckweg 1, 69117 Heidelberg, Germany*
[4]*Théorie, Modélisation, Simulation, SRSMC, UMR CNRS 7565, Université de Lorraine, 57078 Metz, France*
[5]*Departamento de Física, Universidad Nacional del Sur, 8000 Bahía Blanca, Buenos Aires, Argentina*

We present theoretical and experimental fully differential cross sections, in coplanar scattering geometry, for the double ionization of helium by electron impacting at 2 keV. The observed structures for both equal and unequal sharing of the excess energy are analyzed. Although the incident energy could, in principle, be regarded as high enough for the applicability of the first Born approximation in the projectile-target interaction, the experimental cross sections, measured with a COLTRIMS apparatus, show that further orders' effects can be appreciated. The theoretical cross sections are calculated with the generalized Sturmian functions method, which exactly solves the three-body problem that stems from a first-order projectile-target perturbative treatment.

I. INTRODUCTION

The long-range characteristic of Coulomb interactions creates an interesting challenge for theoreticians studying few particle quantum dynamics. With as few as four bodies, as is the case in the double ionization of helium by charged particles, the required solution of the Schrödinger equation cannot be obtained in an exact manner. Whenever the incoming and scattered projectile is fast, the problem is significantly simplified to a more tractable stage: A three-body scattering problem in which exchange effects between the projectile and the target electrons do not come into play.

In the so-called $(e,3e)$ experiments, fully differential cross sections (FDCSs) have been measured for helium at high incident energies of 5.6 keV [1,2], 2 keV [3–5], and 1 keV [6]. Under such kinematical conditions, first-order Born mechanisms with respect to the projectile-target interaction can be expected to be the most important contribution to the cross section. The Orsay group measured FDCSs [7] at lower incident energy, 600 eV, and demonstrated the effect of second-order mechanisms. Their importance was also put in evidence through fourfold differential cross sections [8]. A much lower projectile energy has been considered in Ref. [9], where near-threshold ionization is analyzed.

The experimental FDCSs reported in Refs. [1,2] have the great merit of being on an absolute scale. The data are also those with the most energetic projectiles and are therefore expected to be be well reproduced by first-order Born calculations. Moreover, the momentum transfer was restricted to small values (0.24 a.u. in one kinematical configuration and 0.22 in another one), thus within what is known as dipolar regime (due to the functional similarity of the transition matrix with its photoionization counterpart). The other measurements [3–6] were not presented on absolute scales, but allowed for FDCS shape comparisons to identify and interpret the involved collision mechanisms. The experiments ranged from intermediate momentum transfers ($\approx$0.5 a.u.) [3,6] to high transfers ($\approx$2 a.u.) [4,5], the latter case entering what is known as the impulsive regime.

While it is clear that for the intermediate energies of Refs. [7,8] second-order Born processes are very important,

these effects are, in principle, expected to play a minor role shaping the cross sections for the higher projectile energies, say 1 keV and upwards. Notwithstanding, a first Born model failed to provide a perfect match for the shape of the experimental cross sections in Ref. [6], corresponding to 1.1-keV projectiles. A higher momentum transfer was considered in [4,5], but with 2-keV projectiles. The agreement between experimental and theoretical [convergent close coupling (CCC)] cross sections was clearly acceptable, both for equal and unequal energy sharing. In another study, Dorn *et al.* [3] used 2-keV projectiles but registered collision events with a low-to-intermediate momentum transfer (0.5 a.u.) and undertook only the study of equal-energy configurations.

Overall, there is a lack of studies devoted to unequal energy sharing configurations: The present contribution aims to partially fill this gap. We present and analyze theoretical and relative scale experimental results for the double ionization of helium by 2-keV incident electrons, with momentum transfers of 0.5 and 2.0 a.u. and in coplanar geometry. The experimental data were collected by a COLTRIMS apparatus [5], while the theoretical FDCSs were obtained with the generalized Sturmian functions (GSFs) method [10,11]. This is an *ab initio* approach that has been used so far to solve two- and three-body problems in a numerically exact fashion. In this article we apply it to solve the dynamics of the helium system once it has received a single impact from the projectile, i.e., within a first-order Born projectile-target frame and in a time-independent picture. The complete solution of the continuum three-body Schrödinger equation yields a wave function containing the whole array of allowed processes and internal collisions between the target components. In terms of the multiple scattering expansion by Berakdar *et al.* [12], the GSF formulation contains only the processes which involve a single projectile-target collision, but intratarget collisions are described to all orders. We emphasize here that within the GSF method, the scattering amplitude, and thus the FDCS, is extracted directly from the asymptotic behavior of the continuum three-body scattering solution. Such technique has been recently [13,14] applied to the two $(e,3e)$ experimental kinematic conditions of Refs. [1,2] (small momentum transfers

and equal energy sharing), achieving the first reported shape and magnitude agreement between two theories. In this contribution, the GSF method is used in configurations with larger momentum transfers and with two electrons ejected with both equal and unequal energies.

We have structured the present article as follows. First we describe the experimental setup and the theoretical method. Then we present FDCSs for different excess energies shared equally between the target electrons. Finally, we examine the cross sections under unequal-energy sharing configurations with momentum transfers of 0.5 and 2.0 a.u.

Atomic units ($\hbar = e = m_e = 1$) are used throughout.

II. EXPERIMENTAL SETUP

The experiment was performed with a multielectron recoil-ion momentum spectrometer ("reaction microscope") which has been adapted to the study of electron scattering processes. Details of the experimental method can be found in [5]. It is based on the coincident measurement of the momentum vectors of two slow ejected electrons $\mathbf{k}_2$ and $\mathbf{k}_3$ and the momentum vector of the recoiling ion $\mathbf{K}_{ion}$ emitted in an $(e,3e)$ reaction. Applying momentum conservation, the momentum $\mathbf{k}_f$ of the fast scattered electron or respectively the momentum $\mathbf{q}$ transferred by the scattered projectile is determined,

$$\mathbf{q} = \mathbf{k}_i - \mathbf{k}_f = \mathbf{k}_2 + \mathbf{k}_3 + \mathbf{K}_{ion}, \quad (1)$$

where $\mathbf{k}_i$ is the momentum of the incoming projectile. The momentum resolution with the present extraction fields is about $\Delta \mathbf{k} \approx 0.05$ a.u. for electrons and $\Delta \mathbf{k}_{ion} \approx 0.3$ a.u. for the doubly charged helium ions. The resulting angular resolution for electrons is about $5°$ for 5-eV electrons. The apparatus encompasses a conventional electron gun to produce a pulsed primary beam with a repetition rate of 500 kHz and a pulse length of $\Delta t = 1$ ns. The helium target was provided by a supersonic jet. The helium gas expanded through a 30-μm nozzle and was collimated by two skimmer apertures to form a well localized (2.0 mm diameter) and dense (10^{11} atoms/cm^3) target at the intersection point with the electron beam. Ions and low-energy electrons produced in $(e,3e)$ collisions were extracted to opposite directions by a uniform 2.7 V/cm electric field applied along the apparatus axis and are detected by two-dimensional position sensitive multichannel plates. A solenoidal magnetic field produced by a pair of Helmholtz coils is forcing the slow electrons with nonzero transverse momenta to spiral trajectories. In this way, electrons with energies below 30 eV—and essentially all ions—are detected with the full solid angle of 4π. From the times of flight (TOF) and the measured positions on the detectors the trajectories of the particles can be reconstructed and their initial longitudinal and transverse momentum components are obtained. The 80-mm active diameter electron detector is equipped with a fast delay-line readout and a multihit time-to-digital converter (TDC). Thus, positions as well as arrival times of both electrons emitted in a double ionization event are determined. Due to the combined detector and TDC dead time of about 15 ns, the second electron is registered with reduced efficiency if their flight-time difference falls below 15 ns. This results in a loss of momentum space in the final state for electrons having similar momenta in the longitudinal direction towards the electron detector. In

the experimental cross-section diagrams presented in Sec. IV the regions with reduced detection efficiency are indicated.

III. THEORY

A perturbative formulation in terms of the projectile-target interaction has been proposed for $(e,3e)$ processes [15]. It was applied to the helium double ionization by electron impact, first within a Temkin-Poet version [15] and then to the complete problem [13,14]. In brief, the solution to the full four-body Schrödinger equation is expressed as a perturbative series, the perturbation being the projectile-target interactions. Retaining up to the first order is equivalent to a first-order Born approximation to the projectile-target interactions. The proposal of a plane-wave combination for the projectile, times a—to be determined—function for the target dynamics, $\Phi_{sc}^+(\mathbf{q},\mathbf{r}_2,\mathbf{r}_3)$ leads to the driven equation

$$[h_{He} - E_a]\Phi_{sc}^+(\mathbf{q},\mathbf{r}_2,\mathbf{r}_3)$$
$$= -\frac{4\pi}{q^2}\frac{1}{(2\pi)^3}(Z - e^{i\mathbf{q}\cdot\mathbf{r}_2} - e^{i\mathbf{q}\cdot\mathbf{r}_3})\Phi_i(\mathbf{r}_2,\mathbf{r}_3), \quad (2)$$

where h_{He} is the helium three-body Hamiltonian, $\Phi_i(\mathbf{r}_2,\mathbf{r}_3)$ is the helium ground state ($Z = 2$), and E_a is the energy shared by the two ejected electrons of coordinates $\mathbf{r}_2$ and $\mathbf{r}_3$. The scattering solution to Eq. (2) contains all the processes which can occur to the target electrons, i.e., energy and momentum redistribution among the target components via collisions. A particular emission geometry is directly stimulated or suppressed in $\Phi_{sc}^+(\mathbf{q},\mathbf{r}_2,\mathbf{r}_3)$ via the driven term [14].

Equation (2) is solved in a numerically exact fashion with the GSF approach. Since the formulation together with relevant computational aspects can be found in Ref. [14], only a succinct review is provided hereafter for the sake of providing a self-contained work. The scattering function is expanded in partial waves, i.e., eigenstates of the total angular momentum. As the angular part can be treated analytically, most of the numerical calculations are related to the radial coordinates of both electrons. It is at this stage that the GSF approach comes into play, through an expansion in a GSF set,

$$\Phi_{sc}^+(\mathbf{q},\mathbf{r}_2,\mathbf{r}_3) = \sum_{L,M}\sum_{l_2,l_3}\sum_{n_2,n_3} a_\nu \Theta_\nu(\mathbf{r}_2,\mathbf{r}_3), \quad (3)$$

where the outgoing-type behavior at large values of the coordinates r_2 and r_3 is enforced via the three-body basis elements defined as

$$\Theta_\nu(\mathbf{r}_2,\mathbf{r}_3) = \mathcal{Y}_{l_2l_3}^{LM}(\widehat{\mathbf{r}}_2,\widehat{\mathbf{r}}_3)\frac{S_{n_2l_2}(r_2)}{r_2}\frac{S_{n_3l_3}(r_3)}{r_3}, \quad (4)$$

where the index ν collectively denotes the quantum numbers $\{L,M,l_2,l_3,n_2,n_3\}$ and $\mathcal{Y}_{l_2l_3}^{LM}(\widehat{\mathbf{r}}_2,\widehat{\mathbf{r}}_3)$ are the familiar bipolar harmonics. The $S_{n_2l_2}(r_2)$ and $S_{n_3l_3}(r_3)$ are two-body GSFs which satisfy the equation,

$$\left[-\frac{1}{2}\frac{d^2}{dr^2} + \frac{l(l+1)}{2r^2} + \mathcal{U}(r) - E_s\right]S_{nl}(r)$$
$$= -\beta_{nl}\mathcal{V}(r)S_{nl}(r), \quad (5)$$

with outgoing behavior at large distances [10] and an energy E_s fixed to match the total available for the two emitted electrons, E_a (see Ref. [16]). The auxiliary potential $\mathcal{U}(r)$ is taken equal
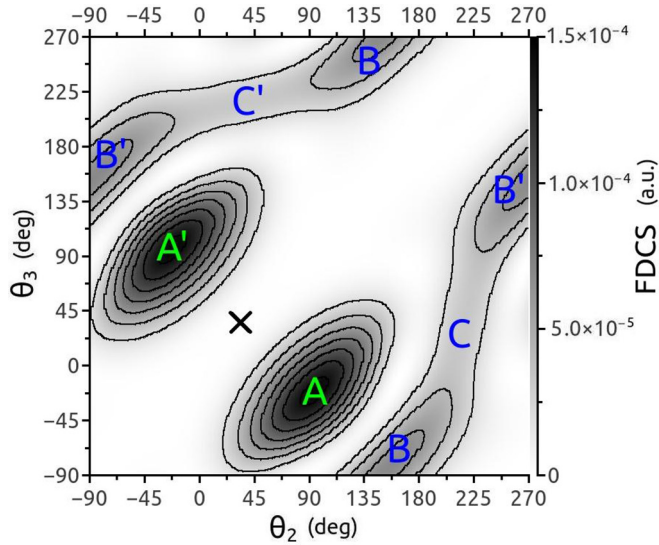
FIG. 1. Theoretical fully differential cross sections, $q = 0.5$ a.u. and $E_a = (25 + 25)$ eV with the binary, recoil, and back-to-back structures labeled by, respectively, A and A', B and B', and C and C'. The momentum transfer is in the direction $\theta_q = 36.61°$ (x mark).

to the helium core potential, while the generating potential $\mathcal{V}(r)$ is one inside the calculation domain (box of radius R) and zero outside. The eigenvalues of Eq. (5) are the β_{nl}, which act as weights of the generating potential. In essence, Eq. (5) is a generalized version of the common radial Schrödinger equation. The three-body basis functions (4) remove the differential operators from the driven equation (2); their linear combination (3) approximates very well the hyperspherical outgoing behavior of the expected solution [16] (an alternative approach, which is under development, uses hyperspherical GSFs [15,17]).

The function $\Phi_i(\mathbf{r}_2, \mathbf{r}_3)$ in (2) stands for an—in principle exact—helium ground-state description. Within our framework it is conveniently calculated with a GSF basis of negative energy that has been demonstrated as sufficiently

precise and computationally efficient [18,19]. In the present contribution we worked with a helium ground-state energy of $-2.903\,48$ a.u. It was observed in Ref. [14] that refining the ground state from $-2.902\,77$ to $-2.903\,34$ a.u. provided only a marginal modification to the calculated FDCS.

We now turn to the computational side of our approach: A projection onto every basis element (4) transforms differential equation (2) into algebraic linear systems for the coefficients a_ν, which are neatly put together as the elements of a vector **a**:

$$[\mathbf{H} - (E_a - 2E_s)\mathbf{S}]\mathbf{a} = \mathbf{b}. \tag{6}$$

The vector **b** contains the projection of the right-hand side of (2) onto each continuum basis element (4). Explicitly, its components are

$$\mathbf{b}_{\nu'} = -\frac{1}{(2\pi)^3}\frac{4\pi}{q^2}\int \mathbf{dr}_2\mathbf{dr}_3\,\Theta_{\nu'}(\mathbf{r}_2, \mathbf{r}_3)$$
$$\times (Z - e^{i\mathbf{q}\cdot\mathbf{r}_2} - e^{i\mathbf{q}\cdot\mathbf{r}_3})\Phi_i(\mathbf{r}_2, \mathbf{r}_3), \tag{7}$$

while the matrix elements for **H** and **S** read

$$\mathbf{H}_{\nu',\nu} = \int \mathbf{dr}_2\mathbf{dr}_3\,\Theta_{\nu'}(\mathbf{r}_2, \mathbf{r}_3)$$
$$\times \left[-\beta_{n_2 l_2}\mathcal{V}(r_2) - \beta_{n_3 l_3}\mathcal{V}(r_3) + \frac{1}{r_{23}}\right]\Theta_\nu(\mathbf{r}_2, \mathbf{r}_3), \tag{8a}$$

$$\mathbf{S}_{\nu',\nu} = \int \mathbf{dr}_2\mathbf{dr}_3\,\Theta_{\nu'}(\mathbf{r}_2, \mathbf{r}_3)\Theta_\nu(\mathbf{r}_2, \mathbf{r}_3). \tag{8b}$$

The calculation of $\Phi_{sc}^+(\mathbf{q}, \mathbf{r}_2, \mathbf{r}_3)$ benefits from the separability of (2) into eigenstates angular momentum sum of electrons 2 and 3, so that one deals with a matrix problem (6) separately for each set of numbers $\{L, M\}$.

Once $\Phi_{sc}^+(\mathbf{q}, \mathbf{r}_2, \mathbf{r}_3)$ is determined, we can extract the collision information from the two-electron continuum asymptotic behavior, which was thoroughly discussed by Kadyrov *et al.* [20],

$$\Phi_{sc}^+(\mathbf{q}, \mathbf{r}_2, \mathbf{r}_3) \underset{\rho\to\infty}{\longrightarrow} (2\pi i)^{1/2}\kappa^{\frac{3}{2}}T_{\tilde{\mathbf{k}}_2, \tilde{\mathbf{k}}_3}\frac{e^{i[\kappa\rho - \lambda_0 \ln(2\kappa\rho) - \sigma_0]}}{\rho^{\frac{5}{2}}}, \tag{9}$$
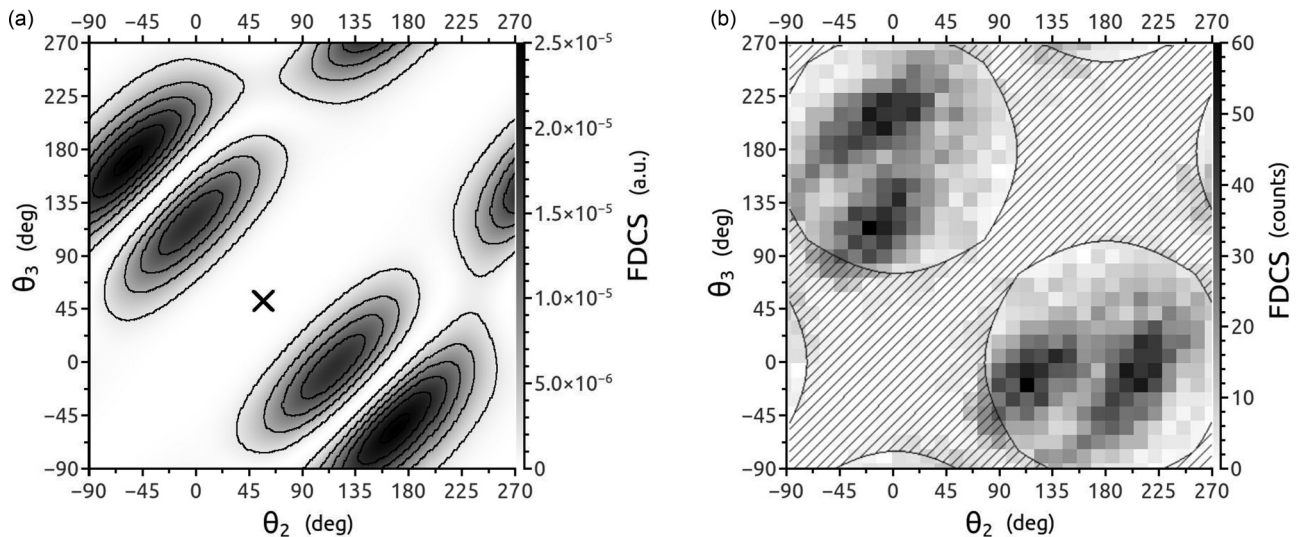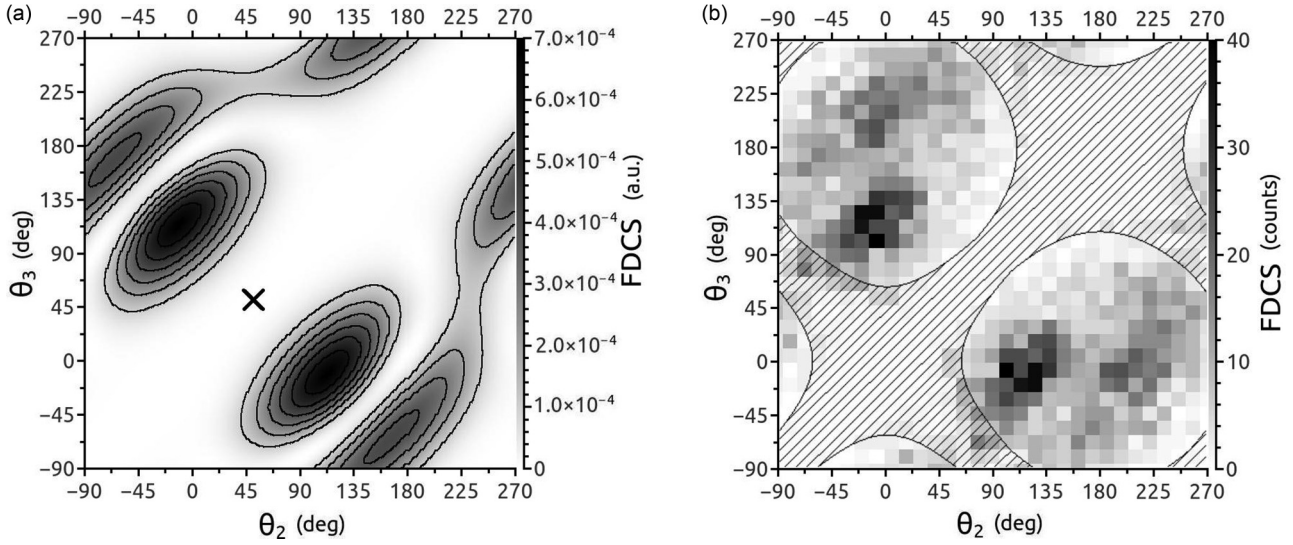

FIG. 2. Fully differential cross sections, $q = 0.5$ a.u. and $E_a = (5 + 5)$ eV: (a) theory and (b) experiment (the hatched area corresponds to reduced detection efficiency). The momentum transfer is angled at $\theta_q = 55.92°$.

FIG. 3. Fully differential cross sections, $q = 0.5$ a.u. and $E_a = (10 + 10)$ eV: (a) theory and (b) experiment (the hatched area corresponds to reduced detection efficiency). The momentum transfer is angled at $\theta_q = 51.62°$.

where $\rho = \sqrt{r_2^2 + r_3^2}$ is the hyperradius, $\kappa = \sqrt{2E_a}$ the hypermomentum, σ_0 a Coulomb phase, and λ_0 a hyperangle-dependent asymptotic Sommerfeld parameter. The coordinate-dependent momenta are defined as $\tilde{\mathbf{k}}_i = \frac{\kappa}{\rho}\mathbf{r}_i$ for ($i = 2,3$) [20,21]. For two electrons escaping with energies E_2 and E_3 in the solid angles $d\Omega_2$ and $d\Omega_3$, the FDCS—for our first-order Born calculation—is defined as

$$\frac{d^5\sigma}{d\Omega_2 d\Omega_3 d\Omega_f dE_2 dE_3} = (2\pi)^4 \frac{k_f k_2 k_3}{k_i} \left| T_{\tilde{\mathbf{k}}_2, \tilde{\mathbf{k}}_3} \right|^2, \quad (10)$$

where the projectile—whose energy $E_f = k_f^2/2$ is determined by total energy conservation—scatters into the solid angle $d\Omega_f$.

Throughout this paper we used radial domains with $R = 50$ a.u. for both electronic radii. From the amplitudes extracted at hyperradii $\rho \approx 47$ a.u. via Eq. (9) we then calculated the

FDCS via (10). We add that, in all cases considered below, we have verified that convergence with respect to the number of partial waves was achieved.

IV. FULLY DIFFERENTIAL CROSS SECTIONS

We find it convenient to split the comparisons between theoretical and experimental results in two sections: the first one devoted to the equal-energy sharing condition and the second one to unequal energy sharing. Indeed, some aspects become appreciable only when the electrons share the excess energy unequally.

We shall display the FDCSs through contour plots, as a function of ejection angles θ_2 and θ_3. Within a first-order Born approximation, the FDCS should be symmetrical with respect to the direction θ_q. Generally, the cross sections present three appreciable types of structure, namely binary,
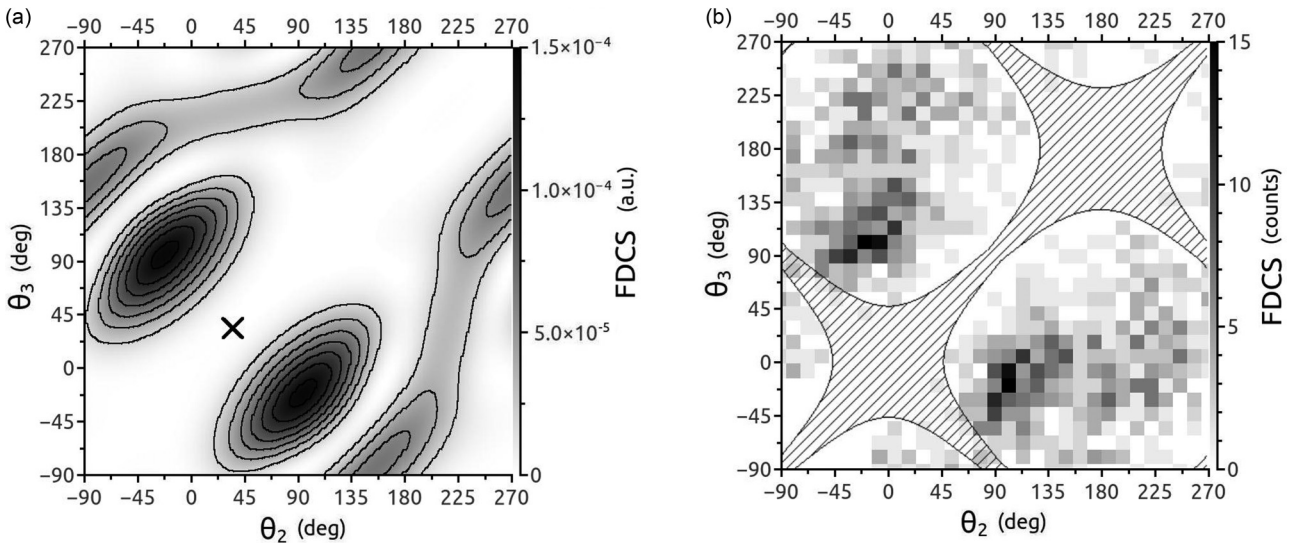

FIG. 4. Fully differential cross sections, $q = 0.5$ a.u. and $E_a = (25 + 25)$ eV: (a) theory and (b) experiment (the hatched area corresponds to reduced detection efficiency). The momentum transfer is angled at $\theta_q = 36.61°$.
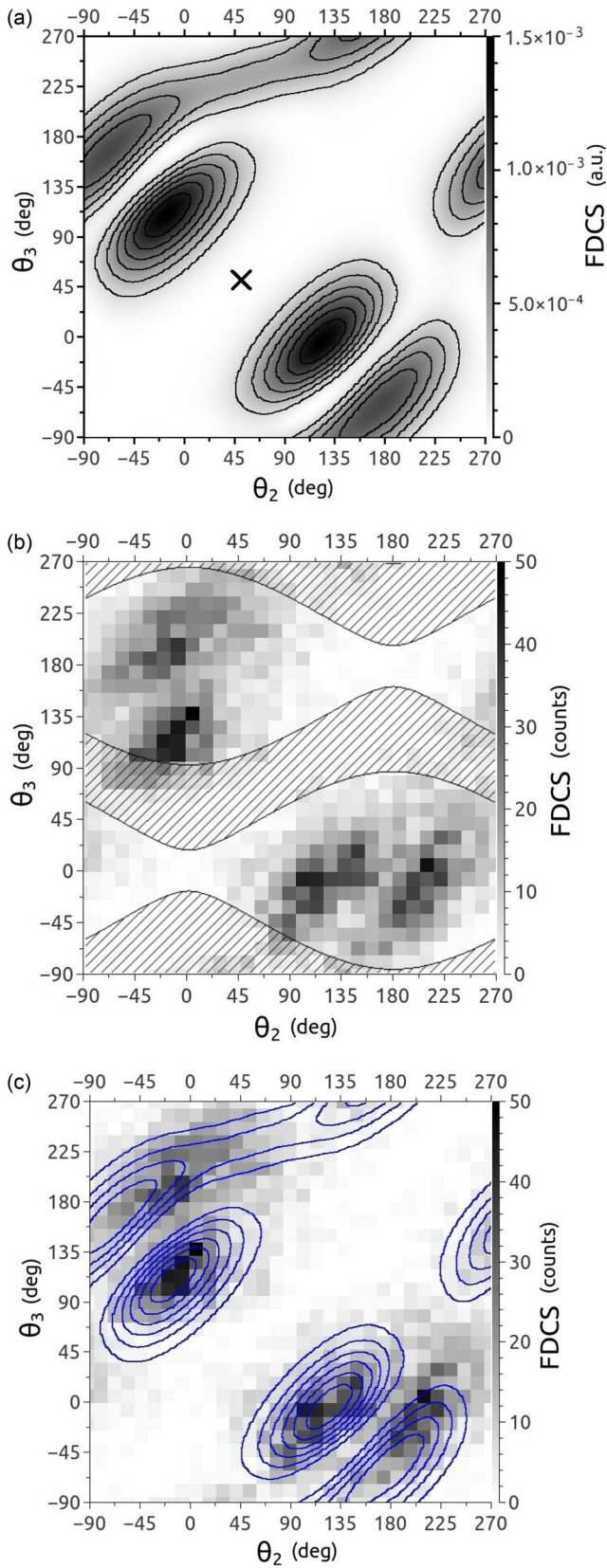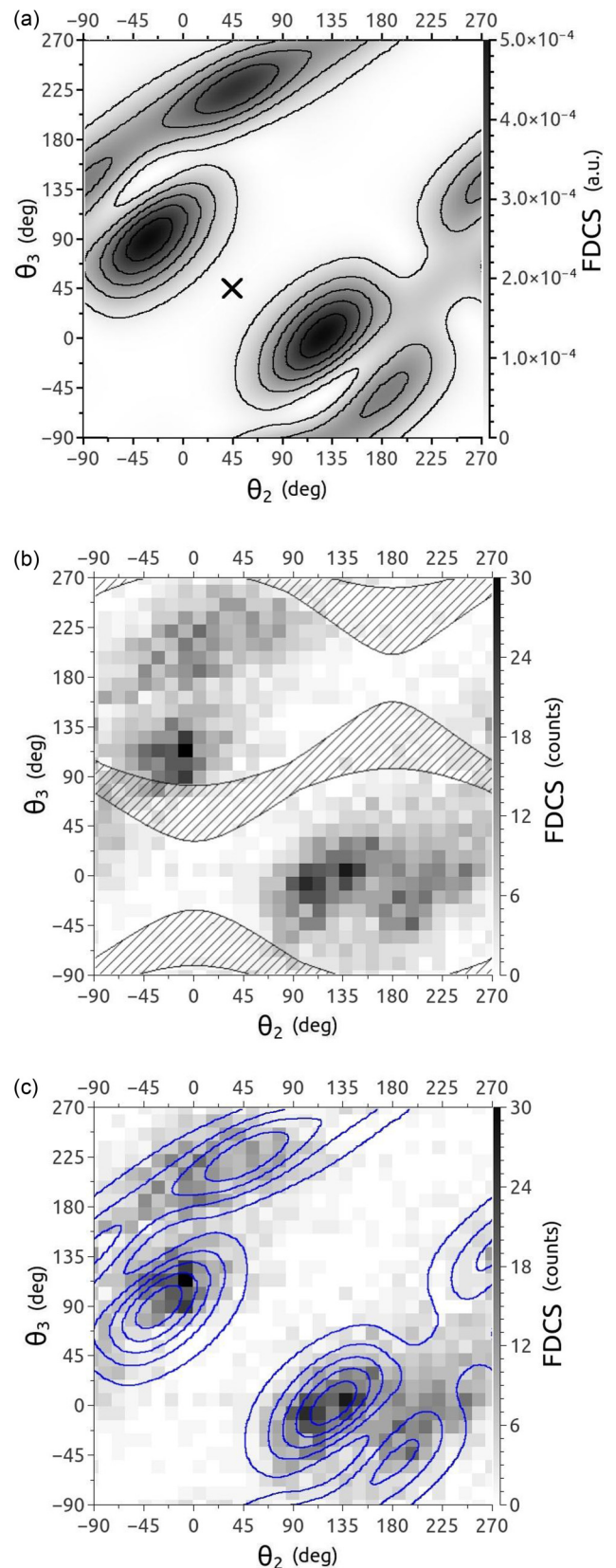
FIG. 5. Fully differential cross sections, $q = 0.5$ a.u. and $E_a = (E_2 + E_3) = (5 + 10)$ eV: (a) theory, (b) experiment, and (c) experiment with superimposed theory (the hatched area corresponds to reduced detection efficiency). The momentum transfer is angled at $\theta_q = 53.80°$.

FIG. 6. Fully differential cross sections, $q = 0.5$ a.u. and $E_a = (E_2 + E_3) = (5 + 25)$ eV: (a) theory, (b) experiment, and (c) experiment with superimposed theory (the hatched area corresponds to reduced detection efficiency). The momentum transfer is angled at $\theta_q = 47.04°$.
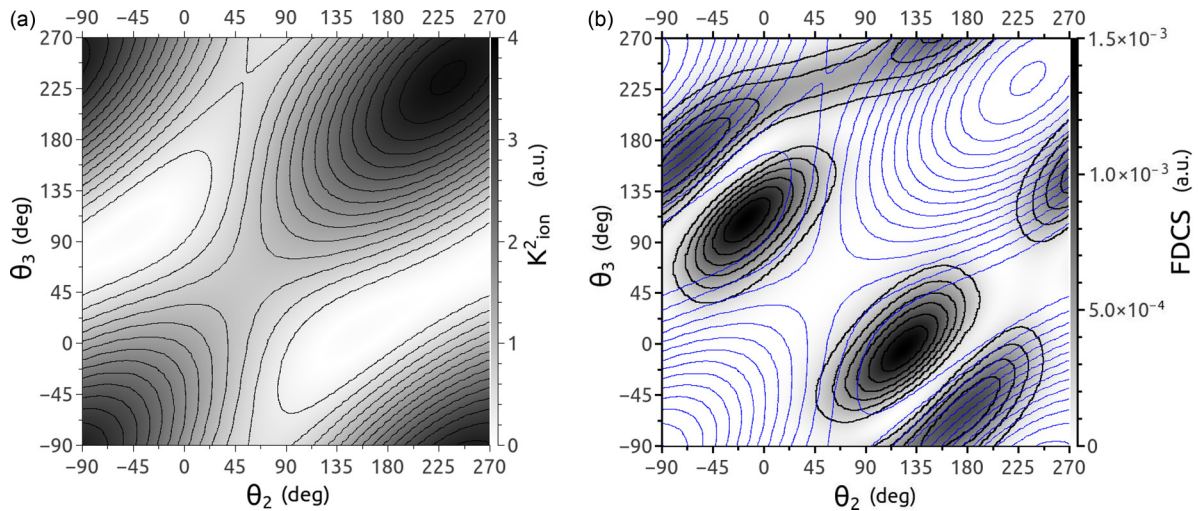
FIG. 7. (a) Squared modulus of the momentum transferred to the core (K_{ion}^2); (b) theoretical FDCS (5 + 10) eV with the K_{ion}^2 contours superimposed.

recoil, and back-to-back peaks; three tags—A, B, C—and their symmetric counterparts—A', B', C'—are placed on their corresponding structures in the explanatory Fig. 1 for an equal-energy-sharing case. Note that in nonsymmetric energy-sharing configurations, the A', B', C' features are no longer mirrored copies of A, B, C.

The binary peak (labeled A and A') characterizes, as its name suggests, a binary collision between the impacted target electron and its partner, which sends them both off to the continuum, the sum of the two ejected electrons' momenta pointing in the $\mathbf{q}$ direction. The recoil structure (tagged B and B') has the momenta sum point towards $-\mathbf{q}$. One way for this to occur is that the impacted target electron recoils off the nucleus and then hits the other one. The recoil emission can also be attained after a pure binary collision, with the addition of a recoil off the core by both electrons. One can expect the recoil process to be more relevant when the electrons have a small excess energy. The back-to-back geometry (labeled C and C' hereafter) implies the emission of the target electrons

in opposite directions. Under the dipolar regime and equal energy sharing, this is greatly suppressed, but if appreciable, they align with the $\pm\mathbf{q}$ directions. This is related to the dot products $\mathbf{q} \cdot \mathbf{r}_2$ and $\mathbf{q} \cdot \mathbf{r}_3$.

A. Equal energy sharing

We begin presenting the FDCSs for three equal-energy con-figurations for $q = 0.5$ a.u. Our experimental and theoretical results are plotted in Figs. 2, 3, and 4.

The theoretical first Born results are, by construction, perfectly symmetric. In order to reduce the statistical error of the experimental data, we exploited the fact that for equal energy sharing between the ionized electrons the cross section is symmetric with respect to a line $\theta_2 = \theta_3$. We have thus accumulated the recorded data in the lower right part of the diagram and mirrored the result along the diagonal of the diagram. An overall good experiment-theory correspondence is observed: The binary peaks A and A', in particular, show an excellent agreement, suggesting that second-order
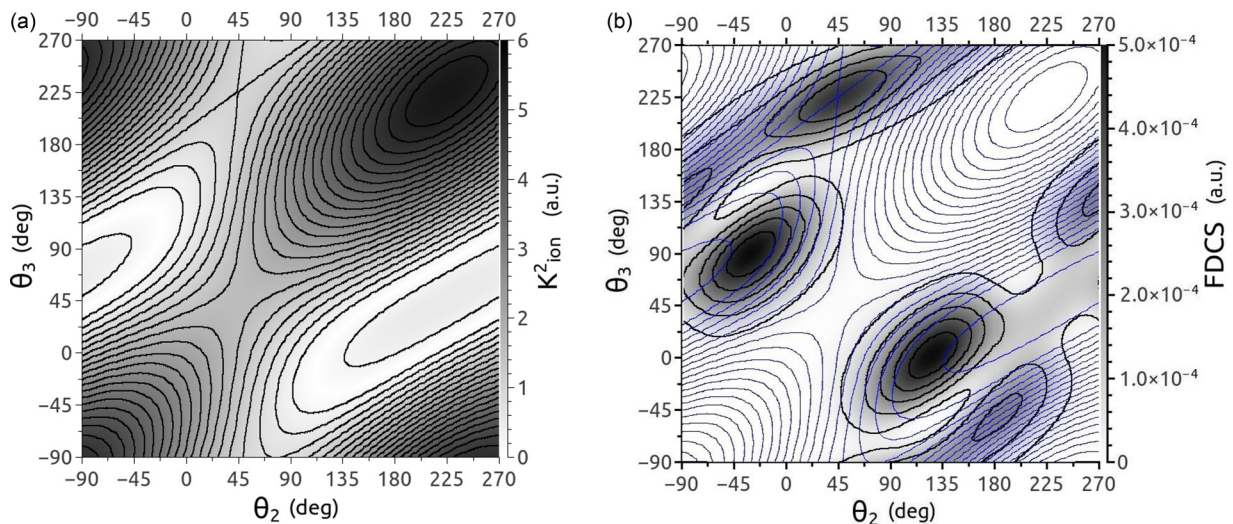

FIG. 8. (a) Squared modulus of the momentum transferred to the core (K_{ion}^2); (b) theoretical FDCS (5 + 25) eV with the K_{ion}^2 contours superimposed.
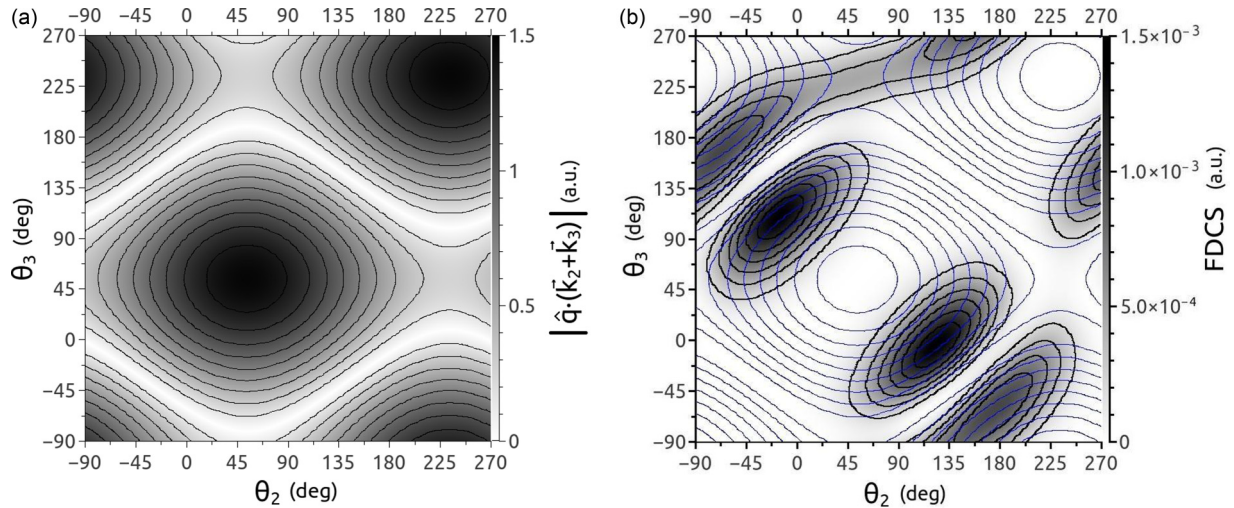
FIG. 9. (a) $|\hat{\mathbf{q}} \cdot (\tilde{\mathbf{k}}_2 + \tilde{\mathbf{k}}_3)|$; (b) theoretical FDCS (5 + 10) eV with the (a) contours superimposed (blue lines).

contributions to the binary emission are negligible. Our results show the peaks A, A' and B, B' aligned as expected from the exponentials in the driven term of Eq. (2). The experimental results hint that, to a degree, further Born mechanisms are playing a role in the collision dynamics. This is evidenced by the B and B' peaks being displaced from their symmetric position described in Fig. 1.

As the excess energy increases, two tendencies can be inferred from both the theoretical and experimental FDCSs presented in Figs. 2, 3, and 4. First, the B, B' structures lose relative height with respect to A, A'. Second, B and B' become more diffuse, merging with a still small but appreciable back-to-back emission. This can be understood with a classical argument, recalling the Rutherford expression for the deflection angle θ_i ($i = 2, 3$) using a very crude model with an effective core charge Z_{eff}:

$$\theta_i = 2 \arctan\left(\frac{-Z_{\text{eff}}}{2E_i b_i}\right). \tag{11}$$

A larger energy value E_i increases the variation of θ_i with respect to the impact parameter b_i, which is, in turn, related

to the *initial position* the electron is extracted from. The distribution that characterizes the initial position is given by the target bound state.

At the lowest ejection energies (Fig. 2) we find that the recoil peak is actually higher than the binary one. The slow electrons of this configuration have a longer time to be affected by the core attractive potential and thus to interact further with it. Picturing it classically, the recoil requires the electrons to perform an orbit around the core before escaping, and this is more likely for lower energies. There is an alternative scenario leading to the same type of structure: First, one of the target electrons receives the energy and momentum imparted by the projectile and, then, it recoils around the core before colliding with the other target electron. Numerically, the GSF solves—in principle exactly—the three-body dynamics to all orders, and thus both aforementioned processes are included and can contribute to the recoil emission.

From Figs. 2, 3, and 4 we can assert that—for faster emitted energies—there is a strong tendency towards a binary emission. Related to the previous classical approach, it can be viewed as if the core attraction is more likely
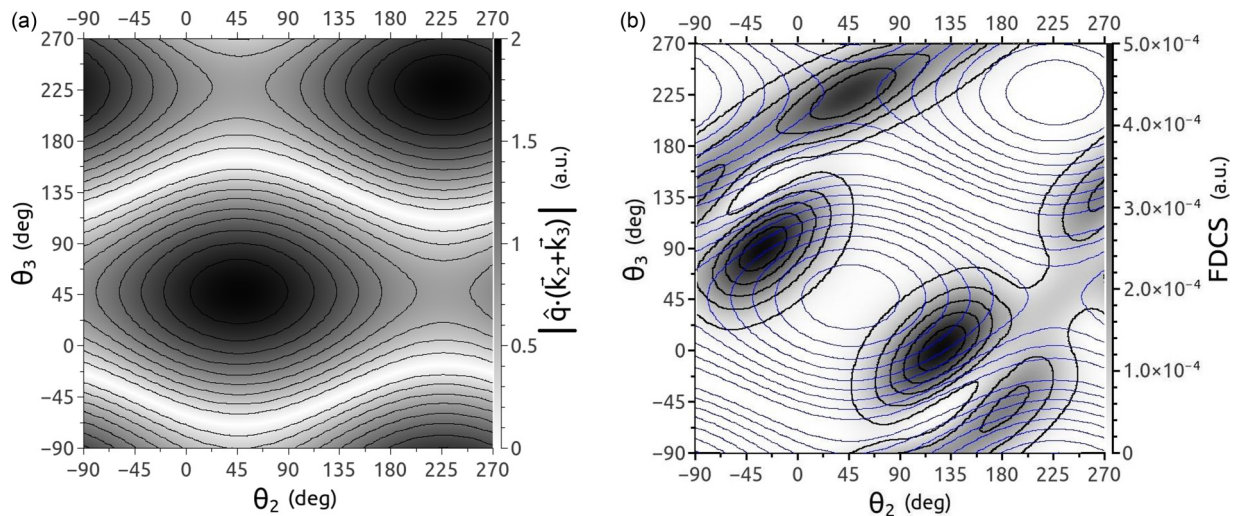

FIG. 10. (a) $|\hat{\mathbf{q}} \cdot (\tilde{\mathbf{k}}_2 + \tilde{\mathbf{k}}_3)|$; (b) theoretical FDCS (5 + 25) eV with the (a) contours superimposed (blue lines).
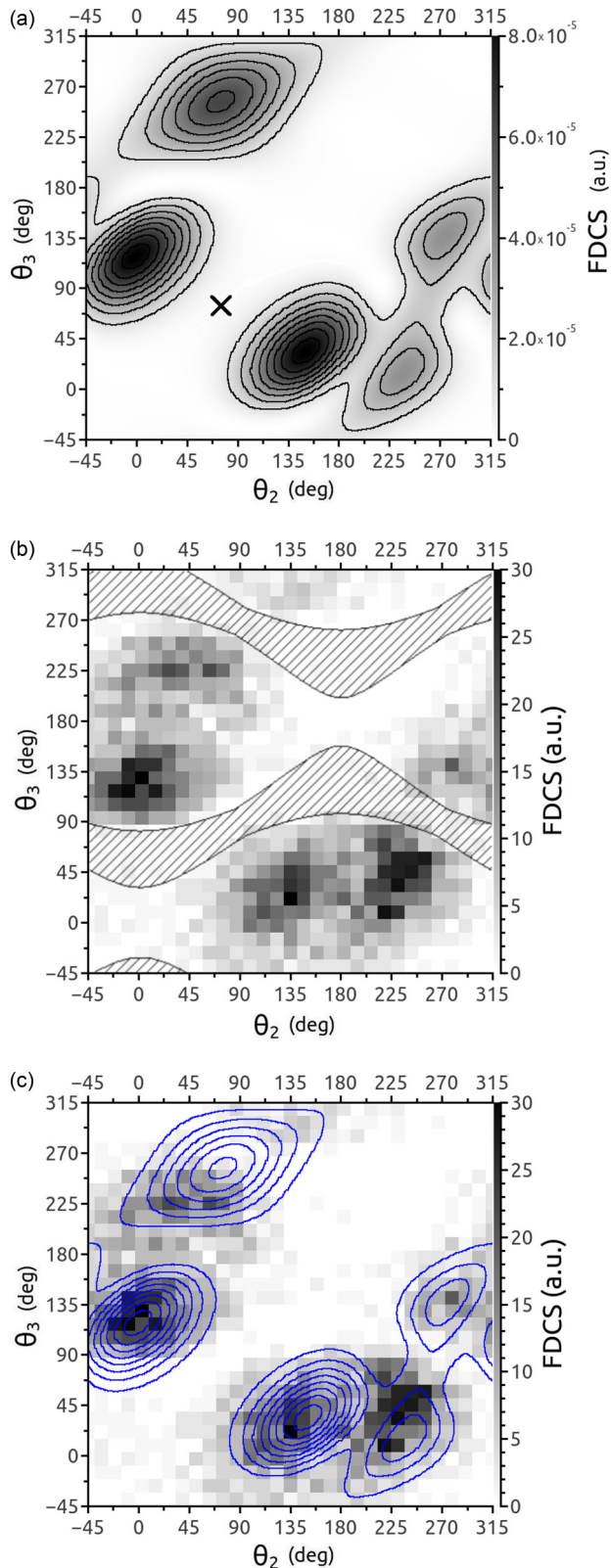
FIG. 11. Fully differential cross section, $q = 2.0$ a.u. and $E_a = (E_2 + E_3) = (5 + 25)$ eV: (a) theory, (b) experiment, and (c) experiment with superimposed theory. The momentum transfer is angled at $\theta_q = 74.76°$.

to play a spectator role, not enforcing any recoil of the electrons.

Let us now comment on the differences observed between the experimental and theoretical FDCSs. The recoil structures look slightly displaced towards the back-to-back emission on the $\pm \mathbf{q}$ directions. One of the electrons is redirected to the forward direction, while the other one is nearly reflected from the upper half plane to the lower half plane (making about the same angle with respect to the incident direction). The $(5 + 5)$-eV case (Fig. 2) makes it evident because the recoil structures are more clearly delimited. Figures 2, 3, and 4 (somewhat less clearly) and even the unequal-energy case (see Fig. 5 later on) show that the experimental recoil structure has one of the electrons shifted towards the forward direction (i.e., $0°$ or $360°$). Since the theoretical FDCSs incorporate the first Born interaction between the projectile and the target, the aforementioned difference can be ascribed to second- or higher-order terms. Therefore, for incident energies as high as 2 keV, second-order effects do have appreciable influence over the FDCS. This statement agrees with the analysis presented in Ref. [3], where similar energy and q regimes were explored for equal-energy sharing.

B. Unequal energy sharing

We now turn to situations in which the ejected electrons depart with different energies, sharing unequally the available excess energy. In this case, the cross sections are no longer expected to be symmetric under a θ_2, θ_3 reflection, and the structures A, B, C (binary, recoil, back-to-back) need not be coincident with A', B', C', respectively. Our theoretical and experimental FDCSs are shown in Figs. 5 and 6 and, again, an overall good correspondence is observed. More intriguing are the theory-experiment comparisons of the recoil and, if present, back-to-back peaks.

In Fig. 5 we can observe that the experimental recoil structures are not coincident with those of the first-order Born calculation. In fact, the way the experimental peaks are displaced is similar to the previously viewed situation for equal-energy configurations. Second-order effects are likely to be responsible for these theory-experiment discrepancies. In turn, back-to-back emission (C, C' peaks) does not seem to be relevant at this energy and momentum transfer configuration, in neither the theoretical nor the experimental cross sections.

The theoretical FDCS presents a C peak that is severely damped, nearly nonexistent. The most obvious candidate accounting for this peak would be the shake-off mechanism. However, it was disregarded in [5] as a viable option to the experimental appearance of the C structure since it would require a more drastically asymmetric energy sharing. Therefore, the presence of the C and C' peaks has then to be due to pure—abrupt—collisions and not to soft relaxations.

For a more pronounced unequal-energy sharing, depicted in Fig 6, we find that there is a back-to-back structure appearing in the theoretical FDCS: an important C' peak but a nonexistent C one. This, although counterintuitive, may be expected from the following theoretical arguments. After interacting abruptly with the projectile, one of the electrons acquires momentum from it. For a back-to-back emission, we would require a number of interactions between the electrons and the core; indeed, a simple head-on interelectronic collision (with or without a previous recoiling off the core) would only make
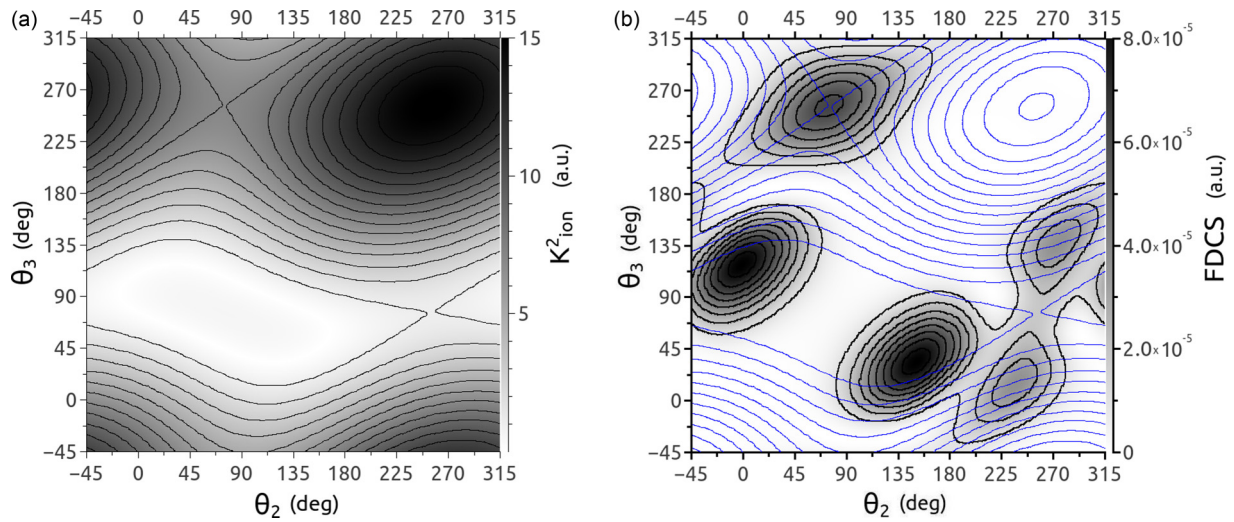
FIG. 12. (a) Squared modulus of the momentum transferred to the core (K_{ion}^2); (b) theoretical FDCS $(5 + 25)$ eV with the K_{ion}^2 contours superimposed.

them swap their momenta, preventing the emission of one of them in the $\pm\mathbf{q}$ direction. The core would have to absorb part of the momentum transferred to the target. However, a very simple—and classical—evaluation of $\mathbf{K}_{ion} = \mathbf{q} - \tilde{\mathbf{k}}_2 - \tilde{\mathbf{k}}_3$ for the kinematics of Figs. 5 and 6 with the fast electron parallel to $\mathbf{q}$ would result in an almost zero momentum transfer to the nucleus (see Figs. 7 and 8). Therefore, this type of back-to-back emission is improbable—small or absent peak C—for the energy and momentum regimes considered. The converse situation, a fast electron emitted towards $-\mathbf{q}$, does, however, incorporate an appreciable amount of momentum transferred to the core and therefore is not prohibited. The binary peaks, on the other hand, do not require a significant participation of the nucleus and therefore can exist in (θ_2, θ_3) directions which imply almost no momentum acquired by the parent core.

There is another argument at play behind the back-to-back phenomenon in Fig. 6, stemming from the dipolar term in the exponentials that appear in Eq. (2). With the position-dependent momenta we obtain for the dipolar limit

$$(Z - e^{i\mathbf{q}\cdot\mathbf{r}_2} - e^{i\mathbf{q}\cdot\mathbf{r}_3}) \approx -i(\mathbf{q}\cdot\mathbf{r}_2 + \mathbf{q}\cdot\mathbf{r}_3)$$
$$= -i\frac{\rho}{\kappa}\mathbf{q}\cdot(\tilde{\mathbf{k}}_2 + \tilde{\mathbf{k}}_3). \quad (12)$$

Figures 9 and 10 show that the back-to-back peak with the fast electron parallel to $\mathbf{q}$ lies accross two *bands* where the process is poorly stimulated in the driven equation (2) and, therefore, loses predominance within the FDCS structures. The C peak, in turn, does not cross these bands.

So far we have described the theoretical FDCS and discussed some arguments behind a particular feature. We now turn to the experimental cross sections depicted in Figs. 5(b) and 6(b). The $(5 + 10)$-eV FDCS presents a shape that resembles the $(5 + 5)$- and $(10 + 10)$-eV ones. There are two clear binary peaks (A, A') which coincide in localization with their theoretical counterparts. The theory suggests that the other structures observable in Fig. 5(a) are due to recoil emission $(B, B'$ peaks). When the energy is shared in a more
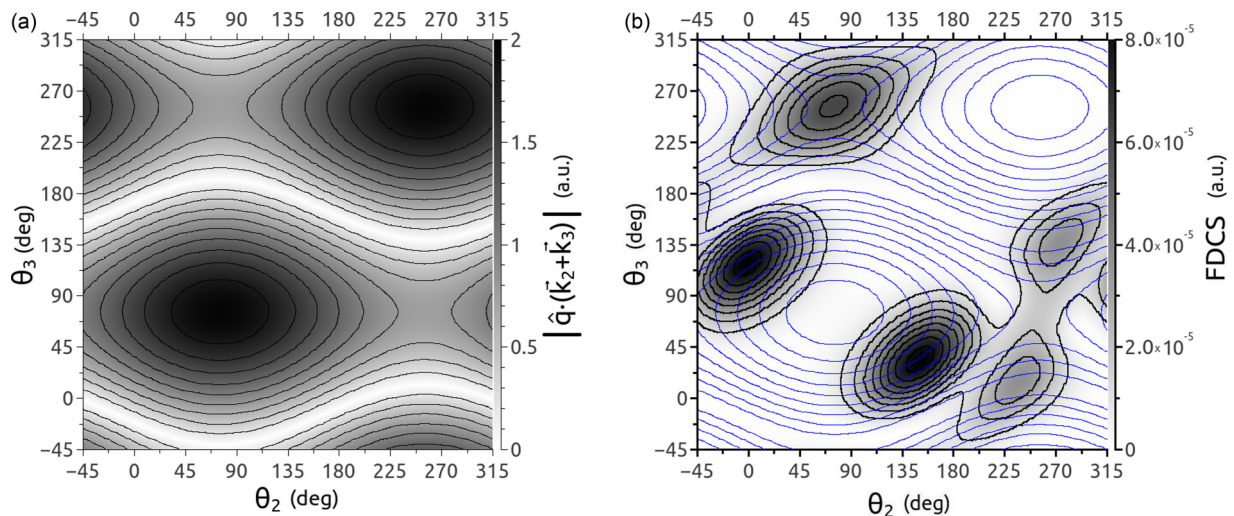

FIG. 13. (a) $|\hat{\mathbf{q}}\cdot(\tilde{\mathbf{k}}_2 + \tilde{\mathbf{k}}_3)|$; (b) theoretical FDCS $(5 + 25)$ eV with the (a) contours superimposed (blue lines).

unequal fashion, the theory-experiment agreement for the binary peaks remains intact. The theory predicts an important C' contribution, and relatively small—but appreciable—B, B' peaks. The C-type emission is minor in the theoretical FDCS. Both experimental recoil and back-to-back structures appear displaced with respect to the first Born ones, with one of the electrons displaced towards the forward direction (i.e., $0°$ or $360°$). The experimental C' peak in Fig. 6(b) seems to be a superposition of displaced first Born peaks C' and B' due to second-order Born interactions.

For comparison, we explored also the larger momentum transfer configuration considered in [5], where the two electrons share 30 eV unequally with a momentum transfer of $q = 2$ a.u. (impulsive regime). The present theoretical calculations are shown in Fig. 11, together with the experimental data (Fig. 3(b) of [5]). Figure 12 compares the FDCS with the K_{ion}^2 contours. When the momentum transfer is increased, the C peak suffers a less important suppression, but at least from the theoretical standpoint it is also damped at the exact point ($\theta_2 = \theta_q + 180°, \theta_3 = \theta_q$). In this impulsive regime, we observe the same type of suppression of the back-to-back peak with the fast electron emitted parallel to $\mathbf{q}$. The first-order calculation this time does contemplate the presence of the back-to-back structure C and the more pronounced C'.

Since at $q = 2$ a.u. we are clearly beyond the dipolar regime, using expansion (12) is out of its strict validity range. Nevertheless, the interpretation for $q = 0.5$ is still present, though to a lesser degree (see Fig. 13). Our theoretical FDCS does not agree with the theoretical CCC calculation (see Fig. 4(b) of Dorn *et al.* [5]). In view of the present evidence, it is possible that the second-order interaction is responsible for the experimental C peak not to be damped as it was seen in our first-order calculations. Second order effects were observed to shift the back-to-back and recoil peaks towards the incidence direction (for one of the ejected electrons).

V. SUMMARY

In this contribution we present a theory-experiment FDCS comparison for the helium double ionization by electron with a relatively high incident energy, 2 keV. While the experimental data sets have a relative scale, they allow for an interesting shape comparison that enables one to determine the relevance of second-order Born effects.

We analyzed first three equal-energy-sharing configurations, with ejection energies of $(5 + 5)$ eV, $(10 + 10)$ eV, and $(25 + 25)$ eV. The binary structures appear completely unaffected by Born orders beyond the first. Theoretically, as the excess energy increases, we expect in the first-order Born a minor appearance of back-to-back emission. The recoil peaks in the three equal energy experimental FDCSs appear to be displaced, having one of the electron's momentum shifted towards $0°$ (or equivalently $360°$), presumably due to second-order projectile-target interactions.

Turning to unequal-energy sharing, we considered two configurations. A $(5 + 10)$ eV sharing and a more unequal $(5 + 25)$ eV case. In both situations the experimental binary peaks are located in accordance with first Born calculations. In the $(5 + 10)$ eV configuration, the displaced recoil peaks suggested by the theory are also observed in the experiments. In the theoretical results, there is a mild expected back-to-back emission, with the slow electron emerging parallel to $\mathbf{q}$, but as it turns out, it is within the level of noise for the experimental results.

The more unequal sharing situation, $(5 + 25)$ eV, makes for a pronounced theoretical back-to-back emission. This peak implies an important emission of the slow (fast) electron parallel (antiparallel) to $\mathbf{q}$.

We discuss two analytical arguments that support our findings. One of them consists of the evaluation of the momentum transferred to the nucleus for all emission angles. The other one considers the dipolar term of the driven equation that defines the wave function.

[1] I. Taouil, A. Lahmam-Bennani, A. Duguet, and L. Avaldi, Phys. Rev. Lett. **81**, 4600 (1998).

[2] A. Kheifets, I. Bray, Lahmamm-Bennani, A. Duguet, and I. Taouil, J. Phys. B **32**, 5047 (1999).

[3] A. Dorn, A. Kheifets, C. D. Schröter, B. Najjari, C. Höhr, R. Moshammer, and J. Ullrich, Phys. Rev. Lett. **86**, 3755 (2001).

[4] A. Dorn, G. Sakhelashvili, C. Höhr, A. Kheifets, J. Lower, B. Najjari, C. Schröter, R. Moshammer, and J. Ullrich, IOP Conf. Proc., Electron Photon Impact Ioniz. Relat. Top. **172**, 41 (2003).

[5] A. Dorn, A. Kheifets, C. D. Schröter, B. Najjari, C. Höhr, R. Moshammer, and J. Ullrich, Phys. Rev. A **65**, 032709 (2002).

[6] A. Lahmam-Bennani, A. Duguet, M. N. Gaboriaud, I. Taouil, M. Lecas, A. Kheifets, J. Berakdar, and C. D. Cappello, J. Phys. B **34**, 3073 (2001).

[7] A. Lahmam-Bennani, A. Duguet, C. Dal Cappello, H. Nebdi, and B. Piraux, Phys. Rev. A **67**, 010701(R) (2003).

[8] A. Lahmam-Bennani, E. M. S. Casagrande, A. Naja, C. D. Cappello, and P. Bolognesi, J. Phys. B **43**, 105201 (2010).

[9] X. Ren, A. Dorn, and J. Ullrich, Phys. Rev. Lett. **101**, 093201 (2008).

[10] G. Gasaneo, L. U. Ancarani, D. M. Mitnik, J. M. Randazzo, A. L. Frapiccini, and F. D. Colavecchia, Adv. Quantum Chem. **67**, 153 (2013).

[11] D. M. Mitnik, F. D. Colavecchia, G. Gasaneo, and J. M. Randazzo, Comput. Phys. Commun. **182**, 1145 (2011).

[12] J. Berakdar, A. Lahmam-Bennani, and C. Dal Cappello, Phys. Rep. **374**, 91 (2003).

[13] M. J. Ambrosio, F. D. Colavecchia, D. M. Mitnik, and G. Gasaneo, Phys. Rev. A **91**, 012704 (2015).

[14] M. J. Ambrosio, F. D. Colavecchia, G. Gasaneo, D. M. Mitnik, and L. U. Ancarani, J. Phys. B **48**, 055204 (2015).

[15] G. Gasaneo, D. M. Mitnik, J. M. Randazzo, L. U. Ancarani, and F. D. Colavecchia, Phys. Rev. A **87**, 042707 (2013).

[16] M. J. Ambrosio, F. D. Colavecchia, D. M. Mitnik, G. Gasaneo, and L. U. Ancarani, J. Phys.: Conf. Ser. **601**, 012004 (2015).

[17] G. Gasaneo and L. U. Ancarani, J. Phys. A **45**, 045304 (2012).

[18] J. M. Randazzo, A. L. Frapiccini, F. D. Colavecchia, and G. Gasaneo, Phys. Rev. A **79**, 022507 (2009).

[19] J. M. Randazzo, L. U. Ancarani, G. Gasaneo, A. L. Frapiccini, and F. D. Colavecchia, Phys. Rev. A **81**, 042520 (2010).

[20] A. S. Kadyrov, A. M. Mukhamedzhanov, A. T. Stelbovics, I. Bray, and F. Pirlepesov, Phys. Rev. A **68**, 022703 (2003).

[21] E. O. Alt and A. M. Mukhamedzhanov, Phys. Rev. A **47**, 2004 (1993).